Extracellular Polymeric Matrix Production and Relaxation under Fluid Shear and Mechanical Pressure in Staphylococcus aureus Biofilms

Hou, Jiapeng; Veeregowda, Deepak H.; van de Belt-Gritter, Betsy; Busscher, Henk J.; van der Mei, Henny C.

Published in:
Applied and environmental microbiology

DOI:
10.1128/AEM.01516-17

Publication date:
2018

AMERICAN SOCIETY FOR MICROBIOLOGY | Applied and Environmental Microbiology®

ENVIRONMENTAL MICROBIOLOGY

Extracellular Polymeric Matrix Production and Relaxation under Fluid Shear and Mechanical Pressure in *Staphylococcus aureus* Biofilms

Jiapeng Hou,[a] Deepak H. Veeregowda,[a,b] Betsy van de Belt-Gritter,[a] Henk J. Busscher,[a] Henny C. van der Mei[a]

[a]University of Groningen and University Medical Center Groningen, Department of Biomedical Engineering, Groningen, The Netherlands

[b]Ducom Instruments Europe BV, Center for Innovation, Groningen, The Netherlands

ABSTRACT The viscoelasticity of a biofilm's EPS (extracellular polymeric substance) matrix conveys protection against mechanical challenges, but adaptive responses of biofilm inhabitants to produce EPS are not well known. Here, we compare the responses of a biofilm of an EPS-producing (ATCC 12600) and a non-EPS producing (5298) *Staphylococcus aureus* strain to fluid shear and mechanical challenge. Confocal laser scanning microscopy confirmed absence of calcofluor-white-stainable EPS in biofilms of *S. aureus* 5298. Attenuated total reflection Fourier transform infrared (ATR-FTIR) spectroscopy combined with tribometry indicated that polysaccharide production per bacterium in the initial adhering layer was higher during growth at high shear than at low shear and that this increased EPS production extended to entire biofilms, as indicated by tribometrically measured coefficients of friction (CoF). CoF of biofilms grown under high fluid shear were higher than those when grown under low shear, likely due to wash-off polysaccharides. Measurement of a biofilm's CoF implies application of mechanical pressure that yielded an immediate increase in the polysaccharide band area of *S. aureus* ATCC 12600 biofilms due to their compression. Compression decreased after relief of pressure to the level observed prior to mechanical pressure. For biofilms grown under high shear, this coincided with a higher percent whiteness in optical coherence tomography-images indicative of water outflow, returning back into the biofilm during stress relaxation. Biofilms grown under low shear, however, were stimulated during tribometry to produce EPS, also after relief of stress. Knowledge of factors that govern EPS production and water flow in biofilms will allow better control of biofilms under mechanical challenge and better understanding of the barrier properties of biofilms against antimicrobial penetration.

IMPORTANCE Adaptive responses of biofilm inhabitants in nature to environmental challenges such as fluid shear and mechanical pressure often involve EPS production with the aim of protecting biofilm inhabitants. EPS can assist biofilm bacteria in remaining attached or can impede antimicrobial penetration. The TriboChemist is a recently introduced instrument, allowing the study of initially adhering bacteria to a germanium crystal using ATR-FTIR spectroscopy, while simultaneously allowing measurement of the coefficient of friction of a biofilm, which serves as an indicator of the EPS content of a biofilm. EPS production can be stimulated by both fluid shear during growth and mechanical pressure, while increased EPS production can continue after pressure relaxation of the biofilm. Since EPS is pivotal in the protection of biofilm inhabitants against mechanical and chemical challenges, knowledge of the factors that make biofilm inhabitants decide to produce EPS, as provided in this study, is important for the development of biofilm control measures.

KEYWORDS FTIR, biofilm relaxation, biofilms, friction, tribochemistry, viscosity

Received 10 July 2017 **Accepted** 11 October 2017

Accepted manuscript posted online 20 October 2017

Citation Hou J, Veeregowda DH, van de Belt-Gritter B, Busscher HJ, van der Mei HC. 2018. Extracellular polymeric matrix production and relaxation under fluid shear and mechanical pressure in *Staphylococcus aureus* biofilms. Appl Environ Microbiol 84:e01516-17. https://doi.org/10.1128/AEM.01516-17.

Editor Andrew J. McBain, University of Manchester

Address correspondence to Henny C. van der Mei, h.c.van.der.mei@umcg.nl.

Bacteria adhere to virtually all industrial and environmental surfaces, including surfaces in the human body. Once adhered, bacteria wrap themselves in a self-produced matrix of extracellular polymeric substances (EPS) (1), hampering penetration of antimicrobials. On surfaces within the human body, such as biomaterial implants and devices, the limited penetration of antibiotics into an established biofilm, together with an immune system that is frustrated by its inability to remove the biomaterial, causes life-threatening biomaterial-associated infections in recipients of biomaterial implants and devices. The EPS matrix not only protects a biofilm against chemical attacks but also yields protection against mechanical forces. The protection offered to biofilm inhabitants against mechanical challenges is largely due to the viscoelastic properties of the EPS matrix (2, 3), which allow relaxation from a deformed state to the original state after relief of the mechanical challenge. Biofilms exposed to a flowing fluid, such as blood, can form streamers with viscoelastic responses under fluid shear on a short timescale, i.e., they relax back to original dimensions within minutes after the flow is arrested (4). In other types of biofilm, full relaxation of deformed biofilms to their original state is impossible or will take up to several hours, which makes it difficult to discriminate between relaxation and growth.

Oral biofilm in the oral cavity, for instance, deforms viscoelastically during powered brushing; when left behind after brushing, its structure has become more open and amenable to antimicrobial penetration both *in vitro* (5) and *in vivo* (6) for at least 1 to 2 h. Accordingly, different relaxation processes that occur simultaneously in a biofilm each have their own characteristic time constants (7). Biofilms can consist of up to 97% water (8), and redistribution of water through a biofilm after deformation occurs within seconds and is obviously fastest due to its small molecular size and low viscosity. Redistribution of water is followed by redistribution of more viscous EPS. Bacteria in a deformed biofilm also seek energetically more favorable positions after deformation, but this process is extremely slow, as demonstrated by time-dependent fluorescence microscopy on deformed *Pseudomonas aeruginosa* biofilms (9).

Attenuated total reflection Fourier transform infrared (ATR-FTIR) spectroscopy can be used to study mechanisms of bacterial adhesion to infrared transparent materials, such as germanium (Ge). Studies on *Caulobacter crescentus* grown directly on Ge crystals using ATR-FTIR spectroscopy suggested use of the amide II band around 1,550 cm^{-1} as a marker for biofilm mass (10). Diffuse reflectance infrared (IR) on *Pseudomonas atlantica* biofilms grown on stainless-steel-associated carbohydrate bands around 1,080 cm^{-1} with EPS revealed that protein and carbohydrate concentrations in biofilms increased with the shear applied during growth (11). Planktonic bacteria in suspension do not produce EPS and EPS production is only initiated upon environmental stimuli, such as adhesion to a surface (12), exposure to antibiotics (13), or possibly fluid shear. Despite seldom being used to study bacterial adhesion, ATR-FTIR spectroscopy is an ideal technique to study the response to environmental stimuli of bacteria growing on Ge crystal surfaces.

The TriboChemist is a newly available instrument combining a sliding-wear tester that can be used to exert mechanical pressure on a surface and FTIR spectroscopy (see Fig. 1). Experiments in the TriboChemist can be carried out on Ge crystals placed in a parallel plate flow chamber, while IR spectra can be measured as a function of time and during exertion of mechanical pressure. The instrument is ideally suited to study the dynamics of EPS matrix production and relaxation in biofilms under fluid shear, as well as during and after mechanical pressure. In addition, the TriboChemist can quantify the coefficient of friction (CoF) between the slider and a biofilm-covered surface.

The aim of the current study is to compare the response of biofilms of an EPS-producing and a non-EPS-producing *Staphylococcus aureus* strain adhering to a Ge crystal to increasing fluid shear or mechanical challenge using the TriboChemist. Use of the TriboChemist uniquely allows determination of the response of a biofilm to fluid shear, effects of mechanical pressure on the production of the EPS matrix, and the dynamics of the relaxation of the biofilm after mechanical pressure.

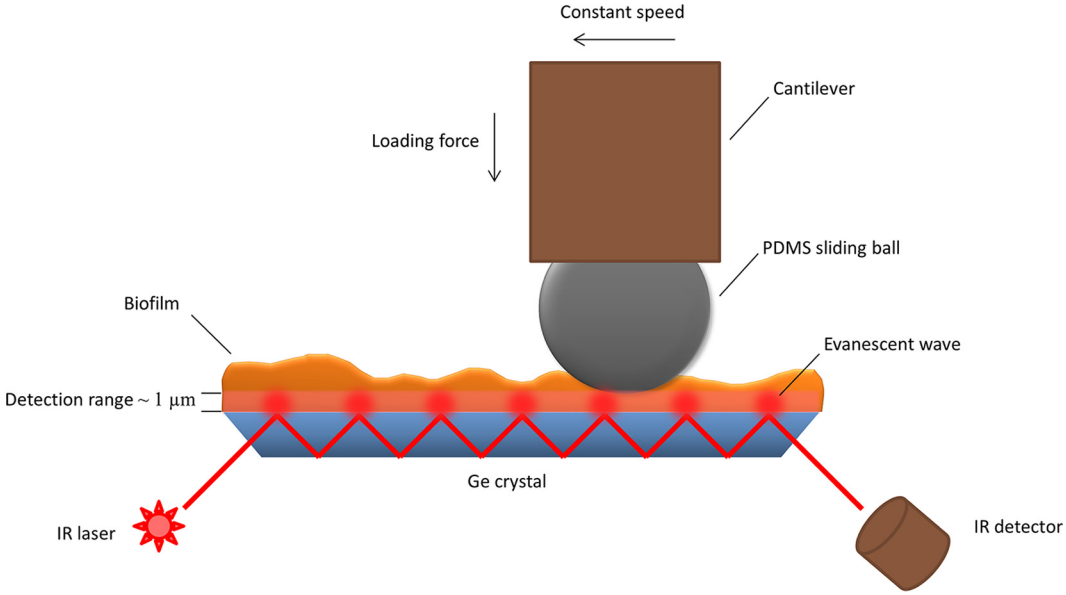

FIG 1 Schematic presentation of the TriboChemist and its possibilities for measuring the lubricity and molecular composition of biofilms grown on a Ge crystal using a combination of a sliding wear tester and FTIR spectroscopy.

RESULTS

Biofilms of non-EPS-producing *S. aureus* 5298 or EPS-producing *S. aureus* ATCC 12600 were grown under low and high shear conditions on a Ge crystal in the parallel plate flow chamber of a TriboChemist and first examined for EPS production using confocal laser scanning microscopy (CLSM) after staining with calcofluor-white and Live/Dead BacLight bacterial viability stain. All biofilms consisted fully of live bacteria (see table inset to Fig. 2), while biofilms of *S. aureus* 5298 (Fig. 2a and b) did not show any of the blue-fluorescent EPS that were abundantly present in biofilms of *S. aureus* ATCC 12600 (Fig. 2c and d). COMSTAT analyses demonstrated 5-fold more EPS production in *S. aureus* ATCC 12600 biofilms grown under high shear than in those grown under low shear (significant at a P value of <0.05). In addition, biofilms of the non-EPS-producing staphylococcal strain grew homogeneously distributed over the Ge crystal surface, while the EPS-producing strain grew more in clusters.

Next, biofilms were subjected to mechanical pressure by sliding a polydimethylsiloxane (PDMS) ball over the biofilm. The friction force experienced by the sliding ball for the bare Ge crystal and biofilm-covered crystals is presented in Fig. 3a. Friction forces were significantly ($P < 0.05$) higher on the bare Ge crystal surface than on the biofilm-covered surfaces, while the EPS-producing *S. aureus* strain ATCC 12600 yielded lower friction forces than the non-EPS-producing *S. aureus* strain 5298. When grown under low shear, CoF of biofilms of the EPS-producing *S. aureus* ATCC 12600 were significantly ($P < 0.05$) lower than those of the non-EPS-producing strain, but when grown under high shear both strains produced biofilms with a similar CoF (see Fig. 3b). Considering the absence of EPS in *S. aureus* 5298 biofilms (compare Fig. 2b), this must be due to different reasons for both strains.

Fourier-transform infrared spectroscopy (FTIR) absorption spectra were taken prior to and during mechanical pressure. Figure 4 shows an example of the IR absorption bands of polysaccharides (Fig. 4a), phosphates (Fig. 4b), and amides (Fig. 4c), as well as of water stretching (Fig. 4d) in a *S. aureus* ATCC 12600 biofilm grown on a Ge crystal surface under high shear (0.79 s^{-1}) prior to and during mechanical shear. The amide absorption band (Fig. 4c) was decomposed in amide I (around 1,643 cm^{-1}) and amide II (around 1,549 cm^{-1}) bands, but the amide I band was not used in the remainder of this study due to its overlap with the water bending band, which also occurred around 1,643 cm^{-1}. The water stretching band (Fig. 4d) was decomposed into two components for bound (around 3,308 cm^{-1}) and free (around 3,469 cm^{-1}) water (14, 15).

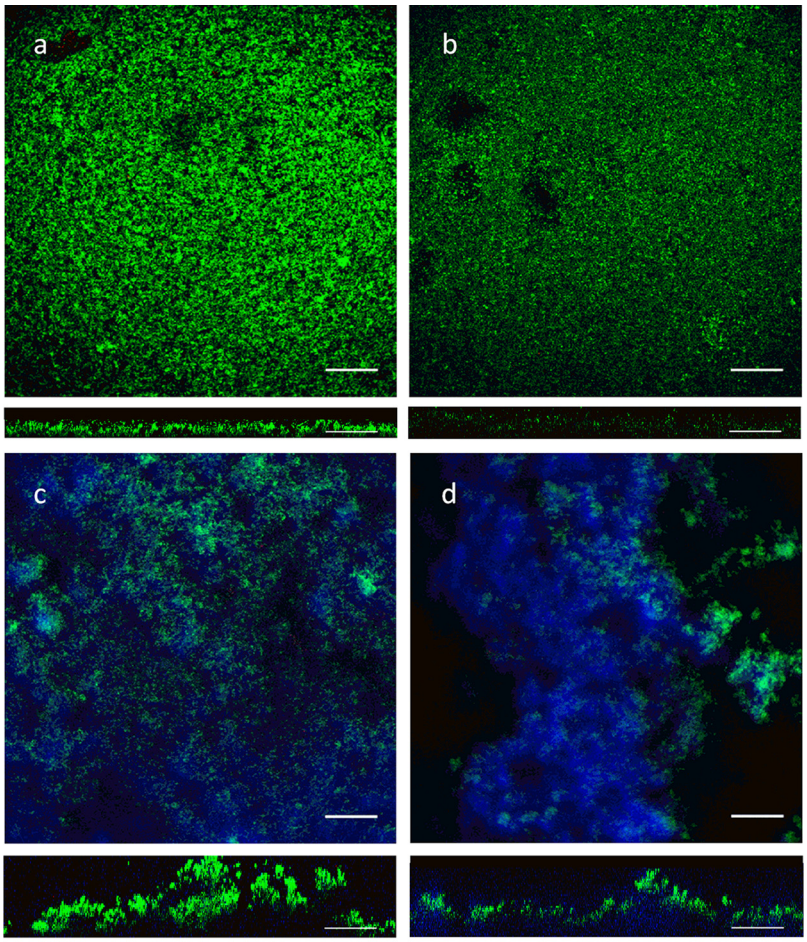

Biovolume ($\mu m^3/\mu m^2$)	5298-LSR	5298-HSR	12600-LSR	12600-HSR
Living bacteria	0.95 ± 0.45	0.36 ± 0.34	0.36 ± 0.10	0.17 ± 0.06
Dead bacteria	0 ± 0	0 ± 0	0 ± 0	0 ± 0
EPS	0 ± 0	0 ± 0	1.07* ± 0.54	5.01* ± 0.93

FIG 2 CLSM images (top views and XZ cross sections) together with biovolumes (table inset) of EPS and of live and dead bacteria in staphylococcal biofilms grown in the parallel plate flow chamber of the TriboChemist under low and high shear and after staining with calcofluor-white and Live/Dead BacLight bacterial viability stain. Live bacteria are green-fluorescent and dead ones are red-fluorescent, while EPS show calcofluor-white blue fluorescence. (a and b) Biofilms of non-EPS producing *S. aureus* 5298 under low (0.16 s^{-1}) (a) and high (0.79 s^{-1}) (b) shear. (c and d) Biofilms of EPS-producing *S. aureus* ATCC 12600 under low (c) and high (d) shear. Data in the table inset are averages over two images ± standard deviations. An asterisk (*) refers to significant differences ($P < 0.05$) between data obtained at low and high shear. Bar, 50 μm.

Absorption band areas and IR absorption band wavenumbers represent the amount and bond stiffness of the corresponding molecules, respectively, and have been plotted in Fig. 5 for the polysaccharide, phosphate, and amide II absorption bands as a function of the CoF measured. Neither the amount of polysaccharides (Fig. 5a) nor the amount of phosphates (Fig. 5b) correlated with the CoF of the biofilms, but biofilms containing more biomass, as evidenced by the amide II absorption band area (11), had significantly ($P < 0.05$) lower CoF (Fig. 5c). Whereas the amount of polysaccharides hardly affected the biofilm CoF, the bond stiffness of the polysaccharides, i.e., the wavenumber of their absorption band, decreased significantly ($P < 0.05$) with increasing CoF (see also Fig. 5a).

The ratio of the polysaccharide over the amide II absorption band areas for the EPS-producing *S. aureus* strain ATCC 12600 was significantly higher (0.44 ± 0.05; $P <$

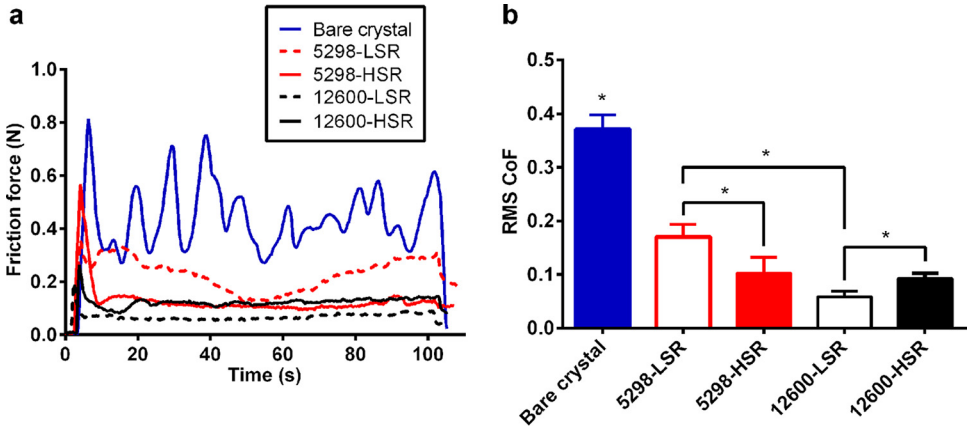

FIG 3 Influence of fluid shear on the friction between *S. aureus* biofilms and a PDMS ball. Friction was measured on biofilms of non-EPS-producing *S. aureus* 5298 (red lines and columns) and EPS-producing *S. aureus* ATCC 12600 (black lines and columns) grown on Ge crystal surfaces under low (0.16 s^{-1}) shear rates (LSR) and high (0.79 s^{-1}) shear rates (HSR), as well as on a wetted, bare Ge crystal without biofilm (blue line and column). (a) Friction forces as a function of time during a single shear stroke with a PDMS ball (sliding speed 0.5 mm/s; loading force 0.45 N). (b) Root mean square (RMS) values of the CoF as averaged over a single stroke (see panel a). Data represent averages over triplicate experiments with separate bacterial cultures and with error bars indicating standard deviations. An asterisk (*) refers to significant differences at $P < 0.05$.

0.05) in biofilms grown under high shear than in those grown under low shear (0.28 ± 0.03). Assuming that the amide II absorption band area represents the number of bacteria in the biofilms, this suggests that shear induces individual organisms to produce more EPS.

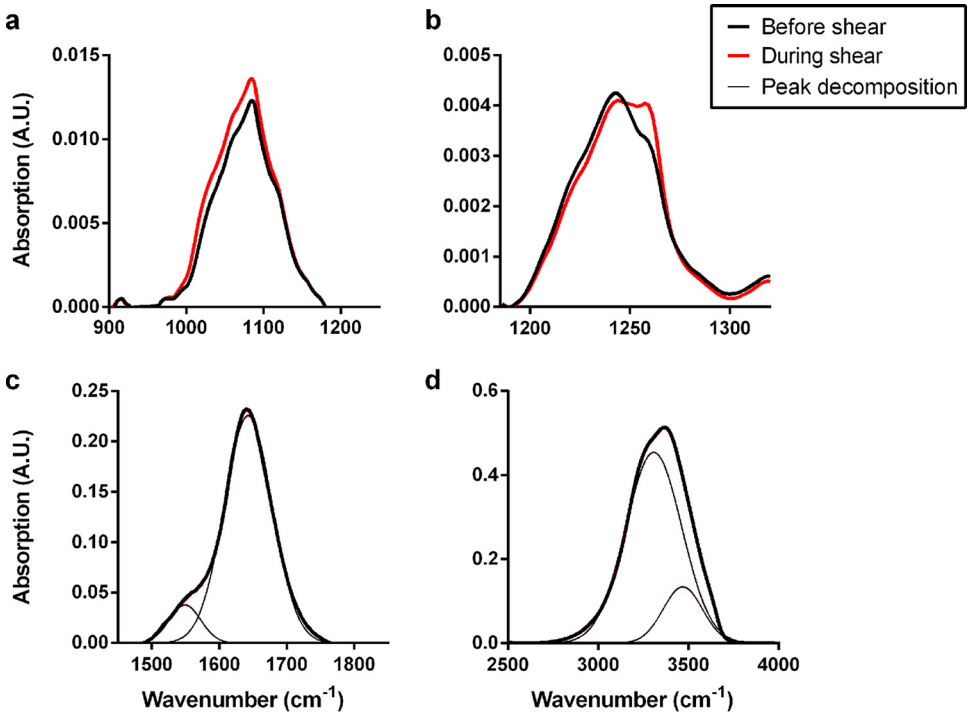

FIG 4 Examples of the FTIR absorption bands in biofilms of EPS-producing *S. aureus* ATCC 12600 grown under high (0.79 s^{-1}) fluid shear on a Ge crystal surface prior to and during mechanical pressure (speed of the sliding PDMS ball, 0.5 mm/s; loading force, 450 mN). (a) Polysaccharide absorption band (950 to 1,200 cm^{-1}), (b) phosphate absorption band (1,150 to 1,310 cm^{-1}), (c) amide absorption band (1,480 to 1,780 cm^{-1}) with the band components at 1,643 and 1,549 cm^{-1} indicating the amide I and amide II bands, respectively. Note that water bending also occurs at 1,643 cm^{-1} and interferes with the amide I band, and (d) water stretching band (2,650 to 3,800 cm^{-1}) with the band components at 3,308 and 3,469 cm^{-1}, indicating bound and free water, respectively. A.U., absorbance units.

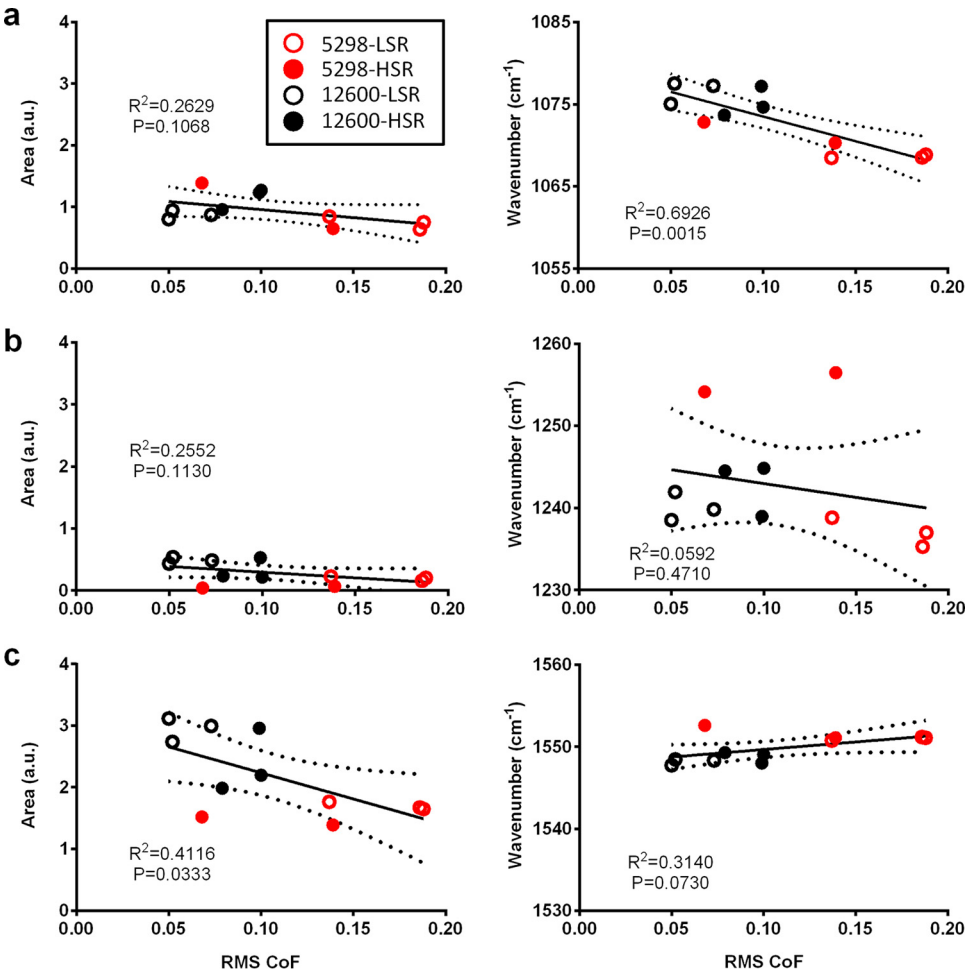

FIG 5 FTIR absorption band areas and wavenumbers of staphylococcal biofilms as a function of the RMS value of their CoF during mechanical deformation for non-EPS-producing *S. aureus* 5298 and EPS-producing *S. aureus* ATCC 12600, grown on Ge crystal surfaces under low (0.16 s^{-1}) and high (0.79 s^{-1}) shear rates. (a) Polysaccharide absorption band (around 1,073 cm^{-1}), (b) phosphate absorption band (around 1,244 cm^{-1}), and (c) amide II absorption band (around 1,549 cm^{-1}). Results of triplicate experiments with separate bacterial cultures are indicated by different symbols of the same type. The solid lines represent the best fit to a linear function with R^2 values indicated, while the dotted lines show the 95% confidence intervals. *P* values indicate significant differences of the slope from zero.

As water is an important transport medium in biofilms and a biolubricant, absorption band areas and wavenumbers for the water stretching band have been plotted in Fig. 6 as a function of the CoF measured. The water O-H stretching band between 2,650 and 3,800 cm^{-1} can be decomposed into absorption bands for bound (around 3,308 cm^{-1}) and free (around 3,469 cm^{-1}) water. CoF increased significantly ($P < 0.05$) with the amounts of both bound (Fig. 6a) and free (Fig. 6b) water. The exact wavenumber of bound water had no influence on the CoF (Fig. 6a), but free water yielded a smaller CoF at lower wavenumbers.

Absorption band areas and wavenumbers were different prior to exertion of mechanical pressure for both strains with respect to the polysaccharide and phosphate bands, but not with respect to the amide or water bands (Fig. 4). Therefore, changes in the polysaccharide and phosphate bands were monitored as a function of biofilm relaxation time after arrest of mechanical pressure (Fig. 7). Relaxation of the polysaccharide band (Fig. 7a) proceeded differently than that of the phosphate band (Fig. 7b). Pressure caused a significant ($P < 0.05$) increase in polysaccharide band area that decreased immediately after relieving pressure in biofilms grown at a high shear rate, regardless of the ability of the strains to produce EPS, and subsequently increased over

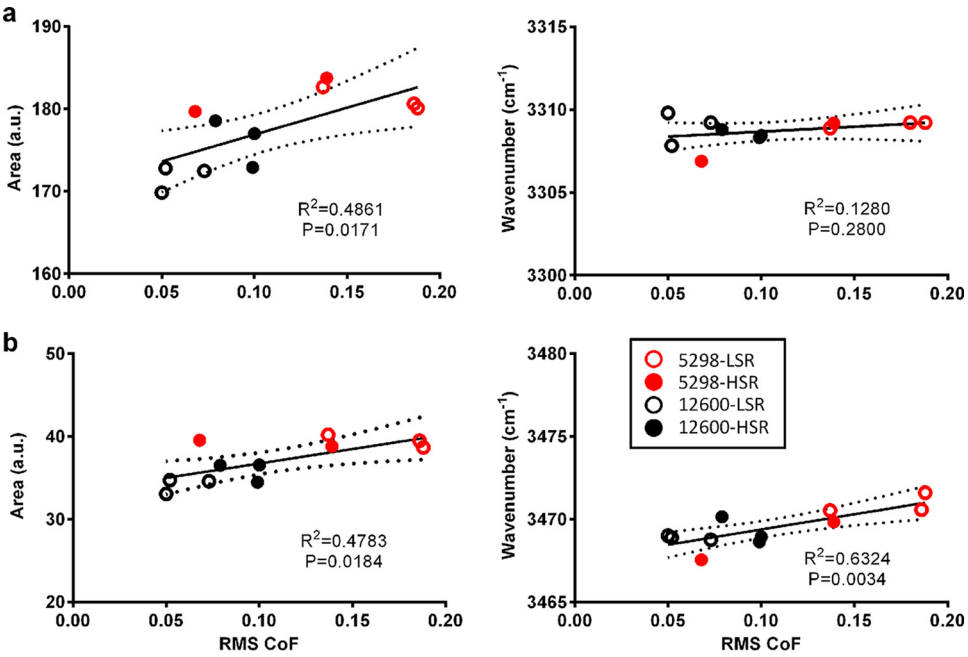

FIG 6 FTIR absorption band areas and wavenumbers for water stretching in staphylococcal biofilms as a function of the RMS value of their CoF for non-EPS-producing *S. aureus* 5298 and EPS-producing *S. aureus* ATCC 12600 strains, grown on Ge crystal surfaces under low (0.16 s^{-1}) and high (0.79 s^{-1}) shear rates. (a) Bound water absorption band (around 3,308 cm^{-1}) and (b) free water absorption band (around 3,469 cm^{-1}). Results of triplicate experiments with separate bacterial cultures are indicated by different symbols of the same type. The solid lines represent the best fit to a linear function with R^2 values indicated, while the dotted lines show the 95% confidence intervals. *P* values indicate significant differences of the slope from zero.

several tens of minutes to the level observed prior to exerting mechanical pressure. Interestingly, *S. aureus* ATCC 12600 biofilms grown under low shear were stimulated by the mechanical pressure exerted during friction measurements to produce more EPS. A decrease in wavenumber during mechanical pressure indicated a weaker bond, but the wavenumber increased almost immediately after relieving pressure to the level observed prior to exerting mechanical pressure. Phosphate bands reacted differently (Fig. 7b), most notably with comparatively small changes for the EPS-producing *S. aureus* strain ATCC 12600, while the non-EPS-producing *S. aureus* strain 5298 showed a strong reaction upon relief of pressure, consisting of a slowly recovering decrease in band area and a strong decrease in wavenumber that continued after relief of pressure.

The differential responses of *S. aureus* ATCC 12600 biofilms grown under low and high shear to mechanical pressure (Fig. 7a) were further examined by visualizing aqueous regions in biofilms prior to, during, and after mechanical pressure using optical coherence tomography (OCT). To this end, biofilms of *S. aureus* ATCC 12600 were grown on glass surfaces under low or high shear, compressed by 33% of their thickness (between 150 and 200 μm) for 300 s between glass plates, and allowed to relax (Fig. 8), which made the biofilm surface appear smoother than in reality (compare CLSM cross sections in Fig. 2c and d). Note that biofilms of *S. aureus* 5298 were too thin (around 40 μm), especially after compression, for OCT imaging. OCT images taken (Fig. 8a) possessed different average whiteness values, indicative of the presence of aqueous regions in the biofilms (16). Biofilms grown under low shear contained less EPS (see Fig. 2, table inset, and Fig. 5a) and appeared more compact from their higher percent whiteness, i.e., their bacterial density (Fig. 8b), than when grown under high shear that stimulated EPS production. Biofilms grown under high shear had higher percent whiteness during compression than prior to compression, indicative of the removal of water upon compression. Upon relaxation, percent whiteness values decreased to their values prior to compression, indicating the return flow of water back into the biofilm, which was also demonstrated by the recovery of its thickness (Fig. 8c).

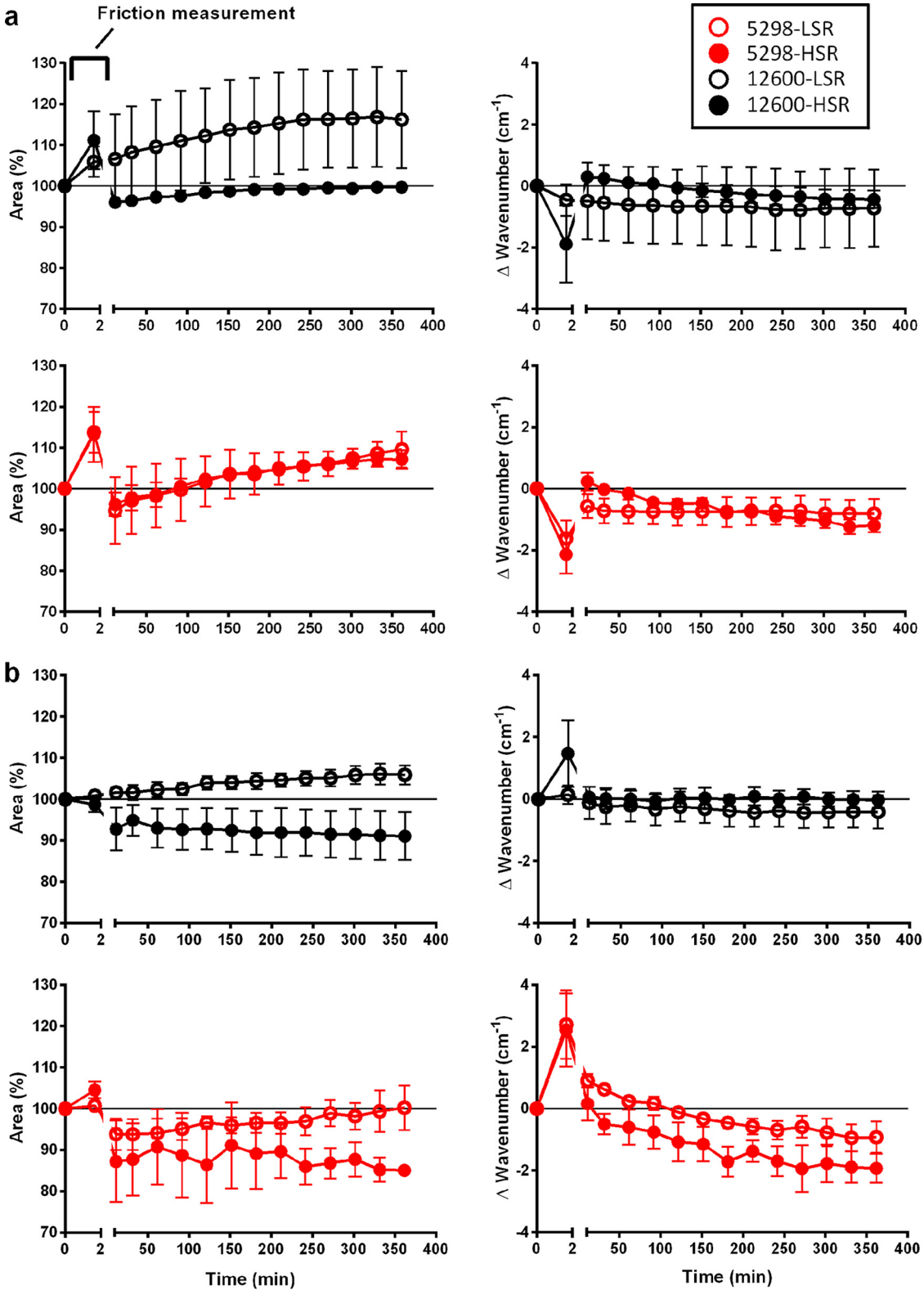

FIG 7 Percentage changes in FTIR absorption band areas and wavenumber shifts as a function of relaxation time after exertion of mechanical pressure on biofilms of non-EPS-producing *S. aureus* 5298 and EPS-producing *S. aureus* ATCC 12600 strains, grown on Ge crystal surfaces under low (0.16 s^{-1}) and high (0.79 s^{-1}) shear rates (speed of the sliding PDMS ball, 0.5 mm/s; loading force, 450 mN). (a) Polysaccharide absorption band (around 1,073 cm^{-1}) and (b) phosphate absorption band (around 1,244 cm^{-1}). Percentage changes in absorption band area and wavenumber shifts were expressed relative to the values observed before exertion of mechanical pressure. Data represent averages over triplicate experiments with separate bacterial cultures and with error bars indicating standard deviations.

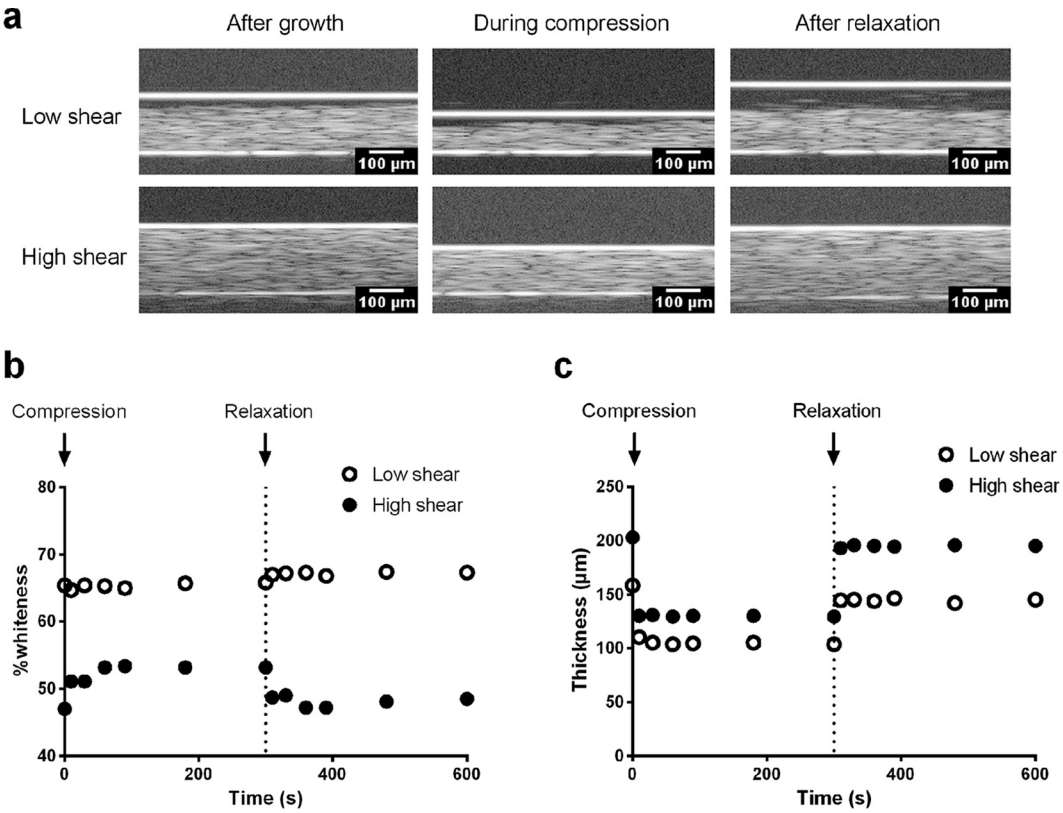

FIG 8 Examples of OCT images of *S. aureus* ATCC 12600 biofilms grown on glass surfaces under low (0.16 s^{-1}) and high (0.79 s^{-1}) shear rates prior to growth, immediately during compression, and after relaxation. (a) OCT images of staphylococcal biofilms. Biofilms are contained and compressed between two glass slides, visible as highly reflecting horizontal lines above and below the biofilm. Images represent a part (300 × 150 pixels) of an entire OCT image, as used to calculate the percent whiteness of a biofilm. (b) Percent whiteness of the biofilms (bacterial density) as a function of time after growth, during compression and relaxation. Percent whiteness represents the whiteness of the biofilm on a scale from 0% (all water) to 100% (all bacteria, no matrix) in the images after correction for the autoscaling of the OCT in images to be compared, which is heavily influenced by reflection from the substratum surface. (c) Thickness of the biofilms as a function of time after growth, during compression and relaxation.

DISCUSSION

Here we show that EPS production and molecular bond stiffness in staphylococcal biofilms are regulated in response to the prevailing fluid shear during growth. Our data suggest that the resulting EPS matrix serves a crucial role in allowing the biofilm to recover from mechanical challenges through in- and outflow of EPS and water upon compression and relaxation.

Biofilm responses to growth under fluid shear. Many of the adaptive responses of adhering bacteria to environmental challenges, including fluid shear, are aimed to facilitate lasting attachment (17). Production of polysaccharides is one of the mechanisms utilized by biofilm inhabitants to provide the biofilm with the ability to adhere more strongly and gain additional cohesive strength (18, 19), as required during growth under high fluid shear. Although diffuse reflectance FTIR spectroscopy has demonstrated that protein and carbohydrate concentrations in *P. atlantica* biofilms increased with applied shear during growth (11), this could not be confirmed in the present ATR-FTIR spectroscopy study. This could be due to the different strains used in both studies, but may also be related to the use of attenuated total reflection (ATR) versus diffuse reflectance spectroscopy. Diffuse reflectance spectroscopy measures the composition of a freeze-dried bulk biofilm sample. In contrast, the ATR-FTIR spectroscopy applied in this study confines itself to a depth of information of one or two micrometers (see also Fig. 1) in a fully hydrated biofilm, comprising only the initially adhering bacteria exposed to fluid shear, i.e., bacteria in the early phases of biofilm growth. Yet,

taking the amide II band area at 1,549 cm^{-1} as a marker for biofilm mass (10) and normalizing the polysaccharide band at 1,073 cm^{-1} by the amount of biofilm mass confirms that the individual bacteria of *S. aureus* ATCC 12600 adhering directly to the crystal surface produced twice as much polysaccharide during growth under high fluid shear conditions as under low fluid shear, while COMSTAT analyses of CLSM images of entire biofilms after calcofluor-white staining revealed a 5-fold greater amount of polysaccharide production under high shear (Fig. 2, table inset).

The molecular mechanisms of increased EPS production under flow can only be speculated upon. Fluid shear forces likely act similarly to the forces involved in bacterial adhesion to substratum surfaces, causing minor deformation of the cell wall in adhering bacteria. The need for EPS production in adhering bacteria is smaller when adhesion forces arising from a substratum surface are large, and accordingly yield less *icaA* gene expression and less production of EPS components such as poly-*N*-acetylglucosamine and extracellular DNA (eDNA) in *S. aureus* ATCC 12600 than when adhering on substrata exerting smaller adhesion forces (12). Since the cell wall, most notably the membrane, houses several environmental sensors, its deformation may present a means for bacteria to probe their environment for the need to produce EPS (20). Fluid shear may act similarly, regulating gene expression and EPS production according to the need to withstand fluid shear forces in order to be able to adhere.

Extension of this increased EPS production by initially adhering bacteria to the bulk of the biofilm is subsequently confirmed by the lower CoF of *S. aureus* ATCC 12600 biofilms compared with the lubricity of *S. aureus* 5298 biofilms (see Fig. 3). However, the slightly higher CoF for EPS-producing *S. aureus* ATCC 12600 biofilm grown under high fluid shear (see Fig. 3) is contrary to the expectation based on increased EPS production in biofilms under high mechanical challenge (Fig. 2). This may be explained by the fact that a high fluid shear washes off soluble and loosely bound EPS from the surface (1). Indeed, FTIR analysis (see Fig. 6) and OCT images (see Fig. 8b) both indicate higher water content in the biofilm grown under high fluid shear, substituting for the EPS flushed away by the fluid shear. Also, biofilms of *Streptococcus oralis* J22 and *Actinomyces naeslundii* TV14-J1 grown under high fluid shear were found to be more "fluffy" (21).

As a totally new and unexpected result, the absorption band around 1,070 cm^{-1} for the non-EPS-producing strain shifted to higher wavenumbers during growth under high fluid shear (see Fig. 5a, right), indicating a stiffer bond. Since biofilms have been described as maintaining themselves under conditions of mechanical challenges by dynamic binding and breaking of weak bonds in the EPS matrix (1), production of stiffer polysaccharides under high fluid shear as reflected by the wavenumber changes of the FTIR absorption band possibly presents a new mechanism for biofilm inhabitants to protect themselves against mechanical challenges.

EPS matrix dynamics under mechanical pressure. The integration of a tribometer together with an FTIR spectrometer in one instrument allows collection of FTIR spectra under mechanical challenge when the tribometer ball is sliding over a biofilm (see Fig. 1). It is known that several processes occur in a mechanically challenged biofilm that range from outflow of water and EPS to the rearrangement of biofilm inhabitants with respect to each other to positions that are more favorable than where they were forced to move to under mechanical pressure (5). Thus, different relaxation processes occur, each with their own characteristic time constants. The mechanical pressure exerted during measurement of biofilm lubricity yielded an immediate increase in the polysaccharide band area of *S. aureus* ATCC 12600 biofilms that decreased within a few minutes after relieving pressure to the level observed prior to mechanical pressure. This is longer than required for water to flow during stress relaxation in a biofilm according to a 3-element Maxwell model, happening within several seconds (5), but it falls with the much longer relaxation time period allocated to the flow of EPS during stress relaxation (5, 22). Also, the relaxation time period of biofilms subjected to fluid shear

was reported to be between 1 and 30 min depending on the hydrodynamic conditions and the type of biofilm (23, 24), similar to the findings of this study.

Actual visualization of rearrangement processes during stress relaxation in biofilms has proven difficult over the years. Peterson et al. (9) visualized the flow of EPS and rearrangement of bacteria in *P. aeruginosa* biofilms during stress relaxation using CLSM; these processes occurred roughly in accordance with relaxation times found using Maxwell analysis of biofilm stress relaxation (5). Visualization of water flow during stress relaxation in biofilms has been done by injection of fluorescent microspheres or fluorescent dyes, followed by CLSM analysis (25), but whether or not microspheres or dyes can cross the biofilm barrier and penetrate into bacterial clusters and EPS matrices in biofilms can be doubted (7). In our study, aqueous regions, possibly with dissolved EPS components, were visualized by whiteness and thickness (Fig. 8b and c) analyses of OCT images. However, whiteness analysis of OCT images is not trivial, as each image is autoscaled by the instrument itself, implying the need to rescale if multiple images are to be compared. The rescaling process applied here is based on normalizing the raw floating points into a fixed 0 to 255 whiteness scale (26, 27) and confirms that for *S. aureus* ATCC 12600 biofilms upon mechanical challenge there is rapid water outflow within seconds, with the water returning back into the biofilm during stress relaxation (see Fig. 8b).

It is of interest that staphylococcal biofilms grown under low shear, during which there was little need to produce large amounts of EPS (see Fig. 5a), continue to produce more polysaccharide for an extended period of time after mechanical pressure (Fig. 7a). Pressure has been described before as a stimulus for bacteria to produce EPS (2, 28). Staphylococci adhering to nanopillared surfaces and exposed to pressure showed EPS patches where nanopillars contacted the cell surface (29). Excessive EPS production was found as well in biofilms exposed to rapidly fluctuating mechanical stress (22). The unique combination of a tribometer and FTIR spectroscope now not only provides additional evidence for pressure-induced EPS production, but demonstrates that pressure-induced EPS production can continue after relief of pressure.

Conclusions. EPS production and molecular bond stiffness in staphylococcal biofilms are regulated in response to fluid shear. EPS matrix dynamics upon mechanical challenge occurs through in- and outflow of EPS and water upon compression and relaxation. Importantly, once mechanically challenged, this can lead to long-term pressure-induced EPS production. Knowledge of factors that control production and quality of EPS in biofilms will allow better control of biofilms under mechanical challenge and better understanding of the barrier properties of biofilms toward mechanical and chemical challenges, most notably antimicrobial penetration. More open biofilms have been found to be more susceptible to antimicrobials both *in vitro* (5) and *in vivo* (30).

Finally, as a distant horizon provided by the current data, biofilms may possibly be applied as an alternative to grease lubricants, although this study was in no way geared toward this possibility and would require the use of harmless bacteria instead of the pathogenic staphylococci used here. Although bacterial lubricants constitute a far horizon, biofilms and their EPS have been considered and applied before in unexpected applications, such as their use to reinforce mortar (31, 32).

MATERIALS AND METHODS

Bacterial strains and culture conditions. *S. aureus* ATCC 12600 and *S. aureus* 5298 were cultured aerobically on tryptone soy broth (TSB; Oxoid, Basingstoke, UK) agar plates at 37°C for 24 h. A single colony was inoculated in 10 ml TSB and grown for 8 h at 37°C. This preculture was used to inoculate a main culture of 200 ml TSB that was grown for 16 h under identical conditions. Bacteria were harvested by centrifugation (5,000 × *g*, 5 min, 10°C) and washed twice with sterile ultrapure water (arium 611 DI water purification system; Sartorius AG, Göttingen, Germany) and resuspended in 10-mM potassium phosphate buffer (pH 7.0). To break bacterial aggregates, the bacterial suspension was sonicated three times for 10 s at 30 W while cooling in an ice/water bath (Vibra-Cell 375; Sonics and Materials Inc., Newtown, CT, USA). The bacteria were then suspended in buffer at a concentration of 1×10^8 bacteria per ml, as determined by using a Bürker-Türk counting chamber.

Biofilm growth. Biofilms were grown on Ge ATR crystals (72 × 10 × 6 mm, angle of incidence 45 degrees; Pike Technology, Wisconsin, USA) in a parallel plate flow chamber (114 × 44 × 2.5 mm). Before each experiment, crystals were cleaned in ultrapure water and isopropanol with a cotton stick, sterilized in 70% ethanol, and air dried overnight at room temperature while covered with a sterile petri dish. After insertion of a crystal into the parallel plate flow chamber and closure of the chamber, an IR background spectrum of the bare crystal was collected (see below for details). Subsequently, the chamber was put on a heating plate and kept at 37°C during perfusion with a staphylococcal suspension (1×10^8/ml) for 2 h at a low (0.16 s^{-1}; Reynolds number, 0.13) or high (0.79 s^{-1}; Reynolds number, 0.63) shear rate to allow adhesion, after which flow was switched to TSB growth medium and biofilm was grown at 37°C for 16 h under the same low or high shear.

Tribochemistry. The TriboChemist (see also Fig. 1) is a novel *in situ* technique that provides information on the dynamics of adsorbed layers during friction (33). The TriboChemist is comprised of an ATR-FTIR spectrometer (Cary 600 Series FTIR spectrometer; Agilent Technologies, Santa Clara, USA) and a tribometer (sliding wear tester TR-17; Ducom Instruments Pvt. Ltd., Bangalore, India). The FTIR spectrometer is used for acquiring IR spectra of the surface layer, while the tribometer measures the CoF.

Lubricity measurements. In the tribometer part, a linear motion drive obtained using a stepper motor (VEXTA Oriental Motor, model PK56W; Oriental Motor Pvt. Ltd., Bangalore, India) enables a reciprocating sliding of a PDMS ball (semihemispherical geometry; radius, 3 mm) over the ATR crystal. A bidirectional load cell (Anyload model 108AA; Anyload Transducer Co. Ltd., Burnaby, BC, Canada) with a maximum loading force of 5 N is used to measure the friction force, F_f. The resolution of the load cell is 0.03% of the maximum load, i.e., 1.5 mN. For the current experiments, stroke length was set to 50 mm and sliding speed to 0.5 mm/s, and loading force was 450 mN. Only single strokes were made, as adjusted using the Winducom 2010 (Ducom Instruments Pvt. Ltd., Bangalore, India) software developed using the LabVIEW platform (National Instruments Corporation, Texas, USA). Friction forces were acquired at a rate of 2 kHz and converted to CoF according to the equation $\text{CoF} = F_f/F_n$, in which F_n is the normal loading force.

Friction force measurements necessitated opening of the flow chamber but were always performed with biofilms fully immersed in ultrapure water. ATR-FTIR spectra of the bare crystal were taken before and after biofilm formation, including during and after friction measurements. Spectra were taken over a wavenumber range from 400 to 4,500 cm^{-1} using an ATR-FTIR spectrometer at a resolution of 4 cm^{-1}. All spectra represent averages from 12 interferograms. Decomposition and fitting of the absorption bands, including the polysaccharide (950 to 1,200 cm^{-1}), phosphate (1,150 to 1,310 cm^{-1}), amide II (1,480 to 1,610 cm^{-1}), and water stretching (2,650 to 3,800 cm^{-1}) bands, were done using the Origin Pro 9.0 program. The amide band and water stretching band were both decomposed into two characteristic absorption bands (representative of amide I/amide II, and bound/free water, respectively), identified through the second derivatives of their IR spectra. Friction measurements were done in triplicate on separately grown biofilms.

CLSM imaging of biofilms. Biofilms grown on the Ge crystal were stained with 250× diluted solution of the Live/Dead *B*acLight bacterial viability kit (1:1 in volume; Molecular Probes, Breda, The Netherlands) at room temperature in the dark for 12 min, followed by a second staining of 0.15 mM fluorescent brightener 28 (calcofluor-white; Sigma-Aldrich Chemie GmbH, Steinheim, Germany) at room temperature in the dark for 3 min. The stained biofilms were then observed under a confocal laser scanning microscope (CLSM; Leica TCS SP2, Heidelberg, Germany) equipped with 40× 0.80 numerical-aperture (NA) water immersion objectives. Bacteria were excited by 488 and 543 nm light and emitted at 495 to 535 nm (green color) for viable bacteria and 580 to 700 nm (red color) for dead bacteria. The EPS of each biofilm was excited by 405 nm light and emitted at 413 to 480 nm (blue color). Image stacks (1,024- × 1,024-pixel resolution) of each biofilm were taken with a step length of 1.5 μm between the top of the biofilm and the Ge crystal. A top view projection was made for each biofilm from the image stacks; these are presented in Fig. 2. The biovolume of live and dead bacteria and EPS in the biofilm was quantitated using the COMSTAT program (34).

OCT imaging of biofilms and whiteness analysis of images. Biofilms were grown on glass microscope slides (76 × 26 mm, Thermo Scientific Menzel; Thermo Scientific, Landsmeer, The Netherlands) in a parallel plate flow chamber (175 × 17 × 0.75 mm). The slides were washed with 2% RBS35 detergent (Fluka Chemie, Buchs, Switzerland) under sonication and rinsed with demineralized water, followed by soaking in methanol and rinsing with demineralized water prior to use. The flow chamber with slides was autoclaved before biofilm growth. The bacterial adhesion and biofilm growth of *S. aureus* ATCC 12600 were kept in the same conditions as the biofilm growth on Ge crystal described above. After 16 h of growth, biofilms were rinsed with 10 mM potassium phosphate buffer (pH 7.0). Then the flow chambers were opened and the slides were kept in the buffer for observation under OCT (Ganymede; Thorlabs Inc., Munich, Germany) with an axial resolution of 5.8 μm and a lateral resolution of 8 μm. A small piece of glass microscope slide (15 × 7.5 mm, Thermo Scientific Menzel; Thermo Scientific Landsmeer, The Netherlands) served as a plunger to induce 33% deformation to each biofilm, which could be controlled by the OCT displacement system (see Fig. S1 in the supplemental material). Deformation was maintained, i.e., the glass plunger was held at its position for 300 s using a homemade position-controlled compression device (1-μm resolution in controlling moving distance). Subsequently, the small glass slide was raised to position before the biofilm was compressed and allowed to relax freely. Biofilms were visualized by OCT B-scan images (cross-sectional tomography, 5,000 × 373 pixels). An OCT video was taken (0.402 s per scan) to record the first 30 s after compression or relaxation. The images from each scan in the video were separated and exported for the analyses. After the video recording, OCT B-scan snapshots were taken every 30 s until 300 s of biofilm deformation or relaxation was reached.

The raw images with floating points of the pixels were normalized into a 0 to 255 range whiteness scale (black and white pixels are indicated as 0 and 255, respectively) (26, 27). Next, the 256-level whiteness scale in an image was reduced to a binary scale, indicating bacteria as white and aqueous regions as black. The threshold whiteness level was determined by the Otsu method (35) by iterating through all possible threshold values and taking the minimal spread in pixel levels on each side of the threshold as the optimum threshold value. Then the biofilm part between the bottom plate and the autodetected biofilm top edge (excluding the nonconnected floating clusters above the biofilm) was sectioned for the calculation of average percent whiteness within the biofilm as based on the whiteness distribution. If a biofilm were composed fully of bacteria, the percent whiteness would be 100% (maximal bacterial density), while if the percent whiteness were to decrease the biofilm would contain more water.

Statistics. All experiments were performed in triplicate with separately prepared bacterial cultures. Significance of differences between experimental groups was analyzed using the Student *t* test, accepting significance at $P < 0.05$.

SUPPLEMENTAL MATERIAL

Supplemental material for this article may be found at https://doi.org/10.1128/AEM.01516-17.

SUPPLEMENTAL FILE 1, PDF file, 0.3 MB.

ACKNOWLEDGMENTS

This work was supported by the University Medical Center Groningen, Groningen, The Netherlands. We acknowledge financial support for the TriboChemist from the Netherlands Organization for Scientific Research (ZonMW91113014).

H. J. Busscher is also director of a consulting company, SASA BV (Thesinge, The Netherlands). D. H. Veeregowda is manager of Ducom Instruments Europe BV (Groningen, The Netherlands). The authors declare no potential conflicts of interest with respect to authorship and/or publication of this article. Opinions and assertions contained herein are those of the authors and are not construed as necessarily representing views of the funding organization or their respective employers. J.H., B.V.D.B.-G., and H.C.V.D.M. declare no competing financial interests.

REFERENCES

1. Flemming H-C. 2011. The perfect slime. Colloids Surf B Biointerfaces 86:251–259. https://doi.org/10.1016/j.colsurfb.2011.04.025.
2. Flemming H-C, Wingender J. 2010. The biofilm matrix. Nat Rev Microbiol 8:623–633. https://doi.org/10.1038/nrmicro2415.
3. Flemming H-C, Wingender J, Szewzyk U, Steinberg P, Rice SA, Kjelleberg S. 2016. Biofilms: an emergent form of bacterial life. Nat Rev Microbiol 14:563–575. https://doi.org/10.1038/nrmicro.2016.94.
4. Klapper I, Rupp CJ, Cargo R, Purvedorj B, Stoodley P. 2002. Viscoelastic fluid description of bacterial biofilm material properties. Biotechnol Bioeng 80:289–296. https://doi.org/10.1002/bit.10376.
5. He Y, Peterson BW, Jongsma MA, Ren Y, Sharma PK, Busscher HJ, Van der Mei HC. 2013. Stress relaxation analysis facilitates a quantitative approach towards antimicrobial penetration into biofilms. PLoS One 8:e63750. https://doi.org/10.1371/journal.pone.0063750.
6. Jongsma MA, Van der Mei HC, Atema-Smit J, Busscher HJ, Ren Y. 2015. *In vivo* biofilm formation on stainless steel bonded retainers during different oral health-care regimens. Int J Oral Sci 7:42–48. https://doi.org/10.1038/ijos.2014.69.
7. Peterson BW, He Y, Ren Y, Zerdoum A, Libera MR, Sharma PK, Van Winkelhoff A-J, Neut D, Stoodley P, Van der Mei HC, Busscher HJ. 2015. Viscoelasticity of biofilms and their recalcitrance to mechanical and chemical challenges. FEMS Microbiol Rev 39:234–245. https://doi.org/10.1093/femsre/fuu008.
8. Zhang X, Bishop PL, Kupferle MJ. 1998. Measurement of polysaccharides and proteins in biofilm extracellular polymers. Water Sci Technol 37:345–348.
9. Peterson BW, Busscher HJ, Sharma PK, Van der Mei HC. 2014. Visualization of microbiological processes underlying stress relaxation in *Pseudomonas aeruginosa* biofilms. Microsc Microanal 20:912–915. https://doi.org/10.1017/S1431927614000361.
10. Nivens DE, Chambers JQ, Anderson TR, Tunlid A, Smit J, White DC. 1993. Monitoring microbiol adhesion and biofilm formation by attenuated total reflection/Fourier transform infrared spectroscopy. J Microbiol Methods 17:199–213. https://doi.org/10.1016/0167-7012(93)90047-L.
11. Mittelman MW, Nivens DE, Low C, White DC. 1990. Differential adhesion, activity, and carbohydrate: protein ratios of *Pseudomonas atlantica* monocultures attaching to stainless steel in a linear shear gradient. Microb Ecol 19:269–278. https://doi.org/10.1007/BF02017171.
12. Harapanahalli AK, Chen Y, Li J, Busscher HJ, Van der Mei HC. 2015. Influence of adhesion force on icaA and cidA gene expression and production of matrix components in *Staphylococcus aureus* biofilms. Appl Environ Microbiol 81:3369–3378. https://doi.org/10.1128/AEM.04178-14.
13. Anderson GG, O'Toole GA. 2008. Innate and induced resistance mechanisms of bacterial biofilms. Curr Top Microbiol Immunol 322:85–105.
14. Eisenberg D, Kauzmann W. 1969. The structure and properties of water. Oxford University Press, London, United Kingdom.
15. Hou J, Veeregowda DH, De Vries J, Van der Mei HC, Busscher HJ. 2016. Structured free-water clusters near lubricating surfaces are essential in water-based lubrication. J R Soc Interface 13:20160554. https://doi.org/10.1098/rsif.2016.0554.
16. Mahdian M, Salehi HS, Lurie AG, Yadav S, Tadinada A. 2016. Tissue characterization using optical coherence tomography and cone beam computed tomography: a comparative pilot study. Oral Surg Oral Med Oral Pathol Oral Radiol 122:98–103. https://doi.org/10.1016/j.oooo.2016.03.021.
17. Tuson HH, Weibel DB. 2013. Bacteria–surface interactions. Soft Matter 9:4368. https://doi.org/10.1039/c3sm27705d.
18. Limoli DH, Jones CJ, Wozniak DJ. 2015. Bacterial extracellular polysaccharides in biofilm formation and function, p 223–247. *In* Ghannoum M, Parsek M, Whiteley M, Mukherjee P (ed), Microbial biofilms, 2nd ed. ASM Press, Washington, DC.
19. Ahimou F, Semmens MJ, Haugstad G, Novak PJ. 2007. Effect of protein, polysaccharide, and oxygen concentration profiles on biofilm cohesiveness. Appl Environ Microbiol 73:2905–2910. https://doi.org/10.1128/AEM.02420-06.
20. Harapanahalli AK, Younes JA, Allan E, Van der Mei HC, Busscher HJ. 2015. Chemical signals and mechanosensing in bacterial responses to their

environment. PLoS Pathog 11:e1005057. https://doi.org/10.1371/journal.ppat.1005057.
21. Paramonova E, Kalmykowa OJ, Van der Mei HC, Busscher HJ, Sharma PK. 2009. Impact of hydrodynamics on oral biofilm strength. J Dent Res 88:922–926. https://doi.org/10.1177/0022034509344569.
22. Shaw T, Winston M, Rupp CJ, Klapper I, Stoodley P. 2004. Commonality of elastic relaxation times in biofilms. Phys Rev Lett 93:98102. https://doi.org/10.1103/PhysRevLett.93.098102.
23. Blauert F, Horn H, Wagner M. 2015. Time-resolved biofilm deformation measurements using optical coherence tomography. Biotechnol Bioeng 112:1893–1905. https://doi.org/10.1002/bit.25590.
24. Tierra G, Pavissich JP, Nerenberg R, Xu Z, Alber MS. 2015. Multicomponent model of deformation and detachment of a biofilm under fluid flow. J R Soc Interface 12:20150045. https://doi.org/10.1098/rsif.2015.0045.
25. Stoodley P, Debeer D, Lewandowski Z. 1994. Liquid flow in biofilm systems. Appl Environ Microbiol 60:2711–2716.
26. Gossage KW, Tkaczyk TS, Rodriguez JJ, Barton JK. 2003. Texture analysis of optical coherence tomography images: feasibility for tissue classification. J Biomed Opt 8:570–575. https://doi.org/10.1117/1.1577575.
27. Balasubramanian M, Bowd C, Vizzeri G, Weinreb RN, Zangwill LM. 2009. Effect of image quality on tissue thickness measurements obtained with spectral domain-optical coherence tomography. Opt Express 17:4019–4036. https://doi.org/10.1364/OE.17.004019.
28. Hizal F, Zhuk I, Sukhishvili S, Busscher HJ, Van der Mei HC, Choi C-H. 2015. Impact of 3D hierarchical nanostructures on the antibacterial efficacy of a bacteria-triggered self-defensive antibiotic coating. ACS Appl Mater Interfaces 7:20304–20313. https://doi.org/10.1021/acsami.5b05947.
29. Hizal F, Choi C-H, Busscher HJ, Van der Mei HC. 2016. Staphylococcal adhesion, detachment and transmission on nanopillared Si surfaces. ACS Appl Mater Interfaces 8:30430–30439. https://doi.org/10.1021/acsami.6b09437.
30. Jongsma MA, Van de Lagemaat M, Busscher HJ, Geertsema-Doornbusch GI, Atema-Smit J, Van der Mei HC, Ren Y. 2015. Synergy of brushing mode and antibacterial use on *in vivo* biofilm formation. J Dent 43:1580–1586. https://doi.org/10.1016/j.jdent.2015.08.001.
31. Farmani F, Bonakdarpour B, Ramezanianpour AA. 2015. pH reduction through amendment of cement mortar with silica fume enhances its biological treatment using bacterial carbonate precipitation. Mater Struct 48:3205–3215. https://doi.org/10.1617/s11527-014-0391-7.
32. Grumbein S, Minev D, Tallawi M, Boettcher K, Prade F, Pfeiffer F, Grosse CU, Lieleg O. 2016. Hydrophobic properties of biofilm-enriched hybrid mortar. Adv Mater 28:8138–8143. https://doi.org/10.1002/adma.201602123.
33. Mangolini F, Rossi A, Spencer ND. 2012. *In situ* attenuated total reflection (ATR/FT-IR) tribometry: a powerful tool for investigating tribochemistry at the lubricant–substrate interface. Tribol Lett 45:207–218. https://doi.org/10.1007/s11249-011-9868-5.
34. Heydorn A, Nielsen AT, Hentzer M, Sternberg C, Givskov M, Ersbøll BK, Molin S. 2000. Quantification of biofilm structures by the novel computer program COMSTAT. Microbiology 146:2395–2407. https://doi.org/10.1099/00221287-146-10-2395.
35. Otsu N. 1979. A threshold selection method from gray-level histograms. IEEE Trans Syst Man Cybern 9:62–66. https://doi.org/10.1109/TSMC.1979.4310076.